Bibliographical reference

Frequency-Domain Edge Diffraction for Finite and Infinite Edges, U. Peter Svensson, Paul T. Calamia and Shinsuke Nakanishi, Acta Acustica **vol. 95** (Number 3), 2009, pp. 568-572

DOI
https://doi.org/10.3813/AAA.918181

Acta Acustica united with Acustica
Vol. 95 (2009) 568 – 572

Short Communications
DOI 10.3813/AAA.918181

Frequency-Domain Edge Diffraction for Finite and Infinite Edges

U. Peter Svensson
Acoustics Research Centre, Department of Electronics and Telecommunications, Norwegian University of Science and Technology, Trondheim, Norway. svensson@iet.ntnu.no

Paul T. Calamia*
Dept. of Computer Science, Princeton University, Princeton, NJ, USA

Shinsuke Nakanishi
Environmental Acoustics Laboratory, Department of Architecture Technology, Hiroshima International University, Kuré 737-0112, Japan

PACS no. 43.20.El

1. Introduction

The classical problem of edge diffraction (ED) from an infinite wedge of arbitrary angle insonified by a point source has various analytical frequency-domain solutions dating back to Macdonald in 1915 [1]. Formulations have also been presented in the time domain and for finite edges, and applications can be found in many areas of study including noise barrier performance [2], room acoustics [3], radiation from loudspeakers [4], and scattering from the ocean surface [5]. Of particular interest here are exact solutions in the time-domain and the frequency-domain. For the former, the Biot-Tolstoy-Medwin method [2, 6] provides the diffraction impulse response from an infinite wedge, and its reformulation by Svensson *et al.* [7] gives the solution for the first-order diffraction from a finite edge as a line integral along the edge. For the latter, Bowman and Senior [8] and Pierce [9] have presented a contour-integral formulation. Their formulations employ a complex integral that requires a suitable integration path, and the complex integration variable does not correspond directly to geometrical factors. Other line integral formulations (see below) as well as the one introduced here, differ by using a physical coordinate as integration variable.

Other line-integral formulations have been described previously in the literature. For example, Embleton [10] presents a solution based on the Kirchhoff approximation (KA), which makes possible the Maggi-Rubinowicz transformation of the Helmholtz-Kirchhoff surface integral into a line integral. A similar KA-based line-integral formulation also has been presented for time-domain calculations by Sakurai and Nagata [11]. Vanderkooy [4] provides a line-integral wedge-diffraction expression based on the high-frequency asymptotic solution from Bowman and Senior [8]. Menounou *et al.* [12] describe the "directive line-source model," an approximate solution based on the integration of infinitesimal secondary sources distributed along a diffracting edge.

The time-domain expression in [7] provides the basis for this work, and it is shown in this paper that the formulation therein can be transformed to provide the exact first-order edge-diffraction solution in the frequency domain for a finite or infinite edge. Furthermore, for an infinite wedge this new formulation is shown to be equivalent to the reference contour-integral solution from [8] and [9] via a transformation of variables. The most important aspect of this new formulation is that it uses the physical coordinate along the edge as integration variable, which implies that finite edges can be handled directly by adjusting the integration range.

Received 1 September 2008,
accepted 26 January 2009.

* Currently working at MIT Lincoln Laboratory, Lexington, MA, USA.

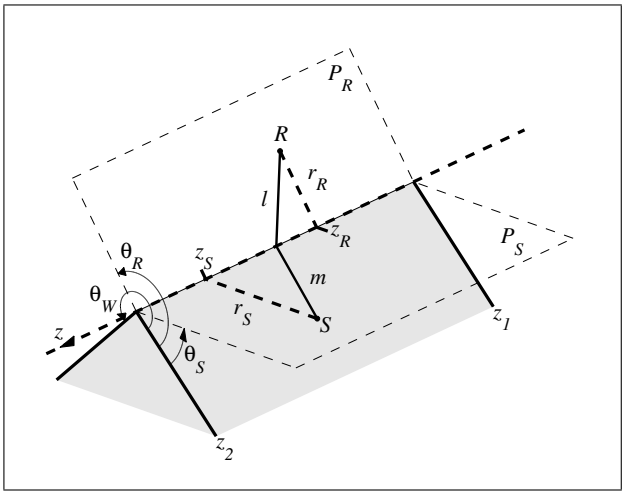

Figure 1. Wedge geometry and edge-aligned cylindrical coordinate system used to describe the source (r_S, θ_S, z_S) and receiver (r_R, θ_R, z_R) positions. P_S and P_R are the planes containing the edge and, respectively, the source and the receiver.

2. The line-integral formulation

2.1. General formulation

Consider an infinite, rigid wedge, with a point source S and a receiver R whose positions are given with edge-aligned cylindrical coordinates (r_S, θ_S, z_S) and (r_R, θ_R, z_R), respectively, as shown in Figure 1. The source signal is defined as $Q(\omega) = \rho_0 A(\omega)/4\pi$ where ρ_0 is the density of air and $A(\omega)$ is the volume acceleration of the point source at the angular frequency ω. Such a source signal implies that the free-field transfer function, or Green's function, is $\mathrm{e}^{-\mathrm{j}kR}/R$ for the sound pressure, where R is the distance from the source to the receiver, $k = \omega/c$ is the wave number and c is the speed of sound. A time function of $\mathrm{e}^{\mathrm{j}\omega t}$ is assumed but suppressed throughout this paper.

The new ED formulation results from a direct Fourier transformation of the time-domain expression presented in [7]. This yields the edge-diffraction transfer function, $H_{diffr}(\omega)$, as a line integral using the z-coordinate along the edge as the integration variable,

$$H_{diffr}(\omega) = -\frac{\nu}{4\pi} \sum_{i=1}^{4} \int_{z_1}^{z_2} \mathrm{e}^{-\mathrm{j}k(m+l)} \frac{\beta_i}{ml} \,\mathrm{d}z, \qquad (1)$$

where $\nu = \pi/\theta_W$ is the wedge index, θ_W is the open (exterior) wedge angle, and m and l are the distances from the source and the receiver, respectively, to an edge point (as seen in Figure 1). The dependence of m and l on z is

$$m = \sqrt{r_S^2 + (z - z_S)^2}, \quad l = \sqrt{r_R^2 + (z - z_R)^2}. \qquad (2)$$

The four β_i, which are also functions of the edge position z, are described below. For a finite wedge, the edge-diffraction solution

is obtained by using the z-coordinate values of the edge endpoints for the integration limits z_1 and z_2. An infinite wedge is modeled with $z_{1,2} = \mp\infty$. The functions β_i, which can be interpreted as edge-source directivity functions, are

$$\beta_i = \frac{\sin(\nu\varphi_i)}{\cosh(\nu\eta) - \cos(\nu\varphi_i)}, \tag{3}$$

where the angles φ_i are

$$\varphi_1 = \pi + \theta_S + \theta_R, \qquad \varphi_2 = \pi + \theta_S - \theta_R,$$
$$\varphi_3 = \pi - \theta_S + \theta_R, \qquad \varphi_4 = \pi - \theta_S - \theta_R, \tag{4}$$

and the auxiliary function η is

$$\eta = \cosh^{-1}\frac{(z - z_S)(z - z_R) - ml}{r_S r_R}. \tag{5}$$

This formulation for η is practical for numerical implementation. However, η can also be written solely as a function of entrance and exit angles towards and from the edge point, thus the interpretation of β_i as directivity functions [7]. For compactness, the dependence of β_i, m, and l on the integration variable z is not written out explicitly throughout the remainder of the paper.

It should be noted that the analytical expressions for the directional edge sources make it possible to derive explicit expressions for first- and even second-order diffraction from some curved edges, such as the circular disc as shown in [7]. See section 2.4 for a further discussion of higher-order diffraction.

2.2. Reflection and shadow boundaries

The integrand in equation (1) comprises only elementary functions and is singular only for certain receiver positions. Specifically, these receiver positions are at the reflection and shadow boundaries (depicted in Figure 2, and hereafter referred to as zone boundaries), *i.e.* the locations where the geometrical-acoustics components (the direct sound and specular reflection) experience discontinuities. At the zone boundaries, the integrand is singular for only one specific value of z. This z-value, z_a, corresponds to the position of the so-called apex point, the point which gives the shortest path from the source to the receiver via the line containing the edge. z_a can be calculated from the radial and axial source and receiver coordinates,

$$z_a = \frac{z_R r_S + z_S r_R}{r_S + r_R}. \tag{6}$$

If z_a is not included in the physical edge, *i.e.* is not in the interval $[z_1, z_2]$, the singularity does not affect the integral and thus ordinary numerical-integration techniques can be used to compute $H_{diffr}(\omega)$.

To avoid the singularity when necessary, it is possible to use an analytical approximation of the integrand in the vicinity of z_a as described in [13]. Such an analytical expression simplifies the numerical integration and offers a formulation which is robust to zone-boundary crossings. For the symmetric case (*i.e.* $z_S = z_R$ or $r_S = r_R$), the integration range is split into two sub-ranges: one in the vicinity of the apex point, up to a point which can be denoted z_{split}, and one for the remainder of the wedge. For such a case the presentation can be simplified by assuming $z_a = 0$ with a wedge that extends symmetrically to an end-point of z_2 so that the integration range can be halved. With these assumptions,

$$H_{diffr}(\omega) = I_1 + I_2 = -2\frac{\nu}{4\pi}\sum_{i=1}^{4}\int_0^{z_{split}} \mathrm{e}^{-\mathrm{j}k(m+l)}\frac{\beta_i}{ml}\,\mathrm{d}z - 2\frac{\nu}{4\pi}\sum_{i=1}^{4}\int_{z_{split}}^{z_2} \mathrm{e}^{-\mathrm{j}k(m+l)}\frac{\beta_i}{ml}\,\mathrm{d}z. \tag{7}$$

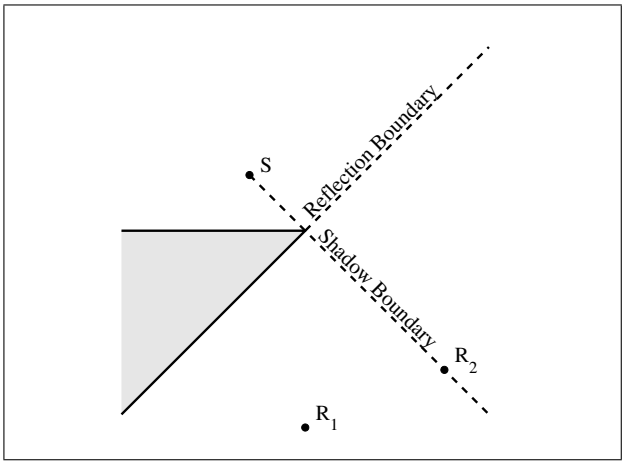

Figure 2. 2D view of the geometry used to produce the results in Figures 3 - 5. For the source: $r_S = 2$ m, $\theta_S = 45°$, $z_S = 0$ m. For receiver R_1: $r_R = 5$ m, $\theta_R = 270°$, $z_R = 0$ m. For receiver R_2: $r_R = 5$ m, $\theta_R = 224.999°$, $z_R = 0$ m. The wedge angle $\theta_W = 315°$. The length of the edge (perpendicular to the page) varies and is given for each set of results.

The second integral, I_2, has no singularities and can be handled with ordinary numerical-integration techniques. The first integral, I_1, is solved using the analytical approximation from [13], with a small modification for the frequency-domain expression. It can be written as

$$I_1 = -2\frac{\nu}{4\pi}\mathrm{e}^{-\mathrm{j}k(m_0+l_0)}\sum_{i=1}^{4}\int_0^{z_{split}} \mathrm{e}^{-\mathrm{j}k(m-m_0+l-l_0)}\frac{\beta_i}{ml}\,\mathrm{d}z, \tag{8}$$

where m_0 and l_0 are distances from the apex point to the source and to the receiver, respectively. Since the purpose of splitting the integration range is only to include the singularity in integral I_1, the point on the edge where the integration range is split can be very close to the apex point such that $m \approx m_0$ and $l \approx l_0$ for I_1. Thus

$$\mathrm{e}^{-\mathrm{j}k(m-m_0+l-l_0)} \approx 1, \tag{9}$$

and then

$$I_1 \approx -2\frac{\nu}{4\pi}\mathrm{e}^{-\mathrm{j}k(m_0+l_0)}\sum_{i=1}^{4}\int_0^{z_{split}}\frac{\beta_i}{ml}\,\mathrm{d}z, \tag{10}$$

and the analytical approximations in [13] can be used directly for the integral. In order to fulfill equation (9), it is required that

$$k(m - m_0 + l - l_0) \ll 1, \tag{11}$$

which leads to

$$z_{split} \ll \sqrt{\frac{2m_0 l_0(m_0 + l_0)}{k(r_S + r_R)^2}}. \tag{12}$$

In addition, the analytical approximations for β_i/ml require that

$$z_{split} \ll m_0, \; z_{split} \ll l_0. \tag{13}$$

For the asymmetric case in which the apex point is included in the wedge, three integration sub-ranges are necessary: one covering a small portion of the edge around the apex point, and one extending from this "apical" region to each of z_1 and z_2.

2.3. Relationship to the contour-integral solution for the infinite wedge

As mentioned in section 1, a related frequency-domain diffraction expression was given in [8] and [9] for the infinite wedge. That formulation is shown below, with some changes of variable names made for easier comparison to the new line-integral method. In particular, the original contour-integral integration variable, t in [8] and s in [9], corresponds to η defined in equation (5). The integration range (typically $-\infty$ to ∞) can be halved because the integrand is even in η. The reference solution is then,

$$H_{diffr}^{ref}(\omega) = -2\frac{\nu}{4\pi}\sum_{i=1}^{4}\int_0^\infty \frac{\mathrm{e}^{-\mathrm{j}k R_{ref}}}{R_{ref}}\beta_i \,\mathrm{d}\eta, \tag{14}$$

where β_i are the same as in equation (3), and

$$R_{ref} = \sqrt{r_S^2 + r_R^2 + (z_R - z_S)^2 + 2\, r_S\, r_R\, \cosh\, \eta}. \tag{15}$$

Comparing equations (1) and (14), equivalence of the two formulations can be established if

$$R_{ref} = m + l, \tag{16}$$

and

$$\frac{\mathrm{d}\eta}{R_{ref}} = \frac{\mathrm{d}z}{ml} \Rightarrow \frac{\mathrm{d}\eta}{\mathrm{d}z} = \frac{R_{ref}}{ml}. \tag{17}$$

To address equation (16), setting $z_S = 0$, without loss of generality, simplifies the derivation somewhat. Squaring both sides of equation (16) leads to the variable

$$f_1 = R_{ref}^2 - (m + l)^2, \tag{18}$$

and the goal is then to show that $f_1 = 0$ (since R_{ref}, m, and l all are positive). Substituting equations (2) and (15) into equation (18) yields

$$\begin{aligned} f_1 &= r_S^2 + r_R^2 + z_R^2 + 2r_S r_R \cosh\, \eta \\ &\quad - \left[\sqrt{r_S^2 + z^2} + \sqrt{r_R^2 + (z - z_R)^2}\right]^2 \\ &= 2r_S r_R \cosh\, \eta - 2z(z - z_R) \\ &\quad - 2\sqrt{r_S^2 + z^2}\sqrt{r_R^2 + (z - z_R)^2}. \end{aligned} \tag{19}$$

In [7], Appendix A, it is shown that

$$\cosh \eta = \frac{ml + z(z - z_R)}{r_S r_R}, \tag{20}$$

which can be inserted in equation (19) resulting in $f_1 = 0$.

Using equation (16), equation (17) can be written as

$$\frac{m + l}{ml} = \frac{d\eta}{dz}. \tag{21}$$

To start the proof of equality, $\frac{d\eta}{dz}$ can be derived using the expression in equation (20),

$$\begin{aligned} \frac{\mathrm{d}\eta}{\mathrm{d}z} &= \frac{r_S r_R}{\sqrt{[ml + z(z - z_R)]^2 - r_S^2 r_R^2}} \\ &\quad \cdot \frac{\frac{\mathrm{d}m}{\mathrm{d}z} l + m\frac{\mathrm{d}l}{\mathrm{d}z} + 2z - z_R}{r_S r_R} \\ &= \frac{\frac{zl}{m} + \frac{(z - z_R)m}{l} + 2z - z_R}{\sqrt{[ml + z(z - z_R)]^2 - r_S^2 r_R^2}} \\ &= \frac{\frac{1}{ml}\left[zl^2 + (z - z_R)m^2 + (2z - z_R)ml\right]}{\sqrt{[ml + z(z - z_R)]^2 - r_S^2 r_R^2}} \\ &= \frac{\frac{1}{ml}\left[z(m + l)^2 - z_R m(m + l)\right]}{\sqrt{[ml + z(z - z_R)]^2 - r_S^2 r_R^2}} \\ &= \frac{\frac{m+l}{ml}\left[z(m + l) - z_R m\right]}{\sqrt{[ml + z(z - z_R)]^2 - r_S^2 r_R^2}}. \end{aligned} \tag{22}$$

Inserting this expression into equation (21), rearranging, and squaring both sides yields the variable f_2 which will be shown to vanish (the involved terms are all positive so the squaring introduces no sign ambiguity),

$$\begin{aligned} f_2 &= \left\{[ml + z(z - z_R)]^2 - r_S^2 r_R^2\right\} - [z(m + l) - z_R m]^2 \\ &= m^2 l^2 + z^2(z - z_R)^2 + 2mlz(z - z_R) - r_S^2 r_R^2 \\ &\quad - \left\{z^2(m + l)^2 + z_R^2 m^2 - 2zz_R m(m + l)\right\} \\ &= m^2\left[l^2 - (z - z_R)^2\right] + z^2\left[(z - z_R)^2 - l^2\right] - r_S^2 r_R^2 \\ &= \left[l^2 - (z - z_R)^2\right](m^2 - z^2) - r_S^2 r_R^2 = 0. \end{aligned} \tag{23}$$

Pierce [9] presents a similar argument by applying a different transformation of variables followed by an inverse Fourier transform to his frequency-domain formulation to arrive at the original (time-domain) Biot-Tolstoy [6] expression for diffraction from an infinite wedge. Chu *et al.* [14] also provide a proof of equivalence between the original Biot-Tolstoy solution and Pierce's contour-integral solution by applying a Fourier transform to the former with a change of integration variable from t to η, followed by a short series of trigonometric and algebraic manipulations.

2.4. Higher-order diffraction

Any internal or external scattering problem with one finite edge must have at least two finite edges that generate diffraction waves. As a consequence, the complete solution must include first-order diffraction waves from all of those finite edges. In addition, there will be multiple-diffraction terms, as has been explored earlier for the time-domain solutions [7, 15]. Finally, combinations of specular reflection and diffraction must be included as well [3, 16]. The solution presented here gives the correct solution for the first-order diffraction contributions, including any number of specular reflection before and after a single diffracting edge. Higher-order diffraction formulations are the topic of further work.

3. Results

One basic geometry has been chosen for comparisons of the new formulation to previous ED solutions. Figure 2 depicts the wedge (in 2D), with one source position, S, and two receiver positions, R_1 and R_2. Furthermore, different edge lengths (perpendicular to the page) are used in the various examples, as specified below. The numerical integration of Eqs. (1) and (14) was computed using the *quadgk* function in Matlab®, which implements adaptive Gauss-Kronrod quadrature. A relative tolerance of 10^{-6} has been used for all calculations.

3.1. Comparison with the reference solution

Equations (1) and (14) were used to compare the new formulation to the reference solution, respectively. Of particular interest

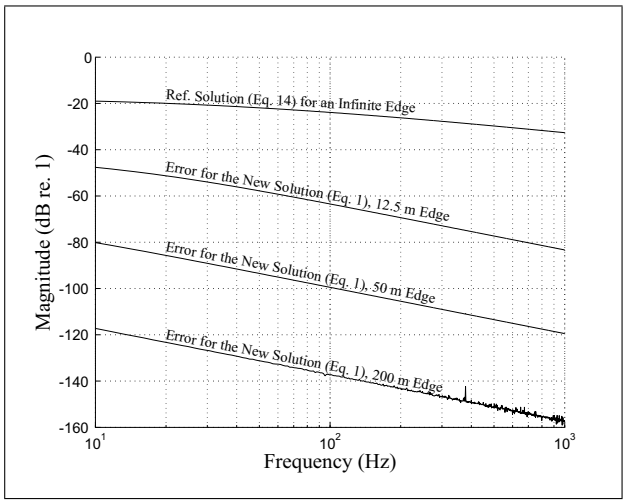

Figure 3. $|H_{diffr}(\omega)|$ calculated with the reference solution for an infinite edge (equation (14)) for the geometry in Figure 2, using receiver R_1. Error for the new formulation (equation (1)) is shown for edges with various lengths, showing the convergence to the reference solution with increasing length.

was the edge length needed in the former to provide a suitable approximation of the infinite edge in the latter. As can be seen in Figure 3, increasing the edge length to 200 m with the new formulation yields results for which the error is approximately 100 dB below the reference solution at low frequencies and decreases with increasing frequency.

3.2. Comparison with the time-domain expression

The new formulation has also been compared to a Fourier transform of the ED impulse-response formulation in [13] for the finite-edge geometry and two receiver positions discussed above and depicted in Figure 2. The edge length was set to 1 m ($z_1 = 0$ and $z_2 = 1$). As described in [7], the use of area sampling to convert the continuous-time expression to a discrete-time IR corresponds to a first-order low-pass filter, and such a low order can result in significant aliasing effects. Therefore, in order to reach a high level of accuracy for the transformed time-domain results, a high sampling frequency must be chosen. Figure 4 presents the new method as the reference magnitude spectrum ($|H_{diffr}(\omega)|$) along with the spectral error associated with Fourier-transformed time-domain calculations using sampling frequencies of 384, 192, 96, and 48 (Figure 4a only) kHz.

As can be seen in Figure 4a for receiver R_1, the error decreases as expected when the sampling frequency is increased, indicating that the dominant source of error is the aliasing mentioned above. For each sampling frequency, the error increases approximately 6 dB per octave due to the first-order nature of low-pass filtering due to area sampling. The ripple seen in the frequency-domain solution is caused by the finite length of the edge.

In Figure 4b, results are shown for receiver R_2 which is very close to the shadow boundary. The reference magnitude spectrum is nearly flat, corresponding to the Dirac-like behavior of the diffraction in the time domain for such receiver positions. The error is significantly higher in this case, also due to the pulse-like characteristics of the impulse response near the zone boundaries.

4. Conclusions

A new frequency-domain, line-integral formulation for the diffraction from a wedge insonified by a point source has been

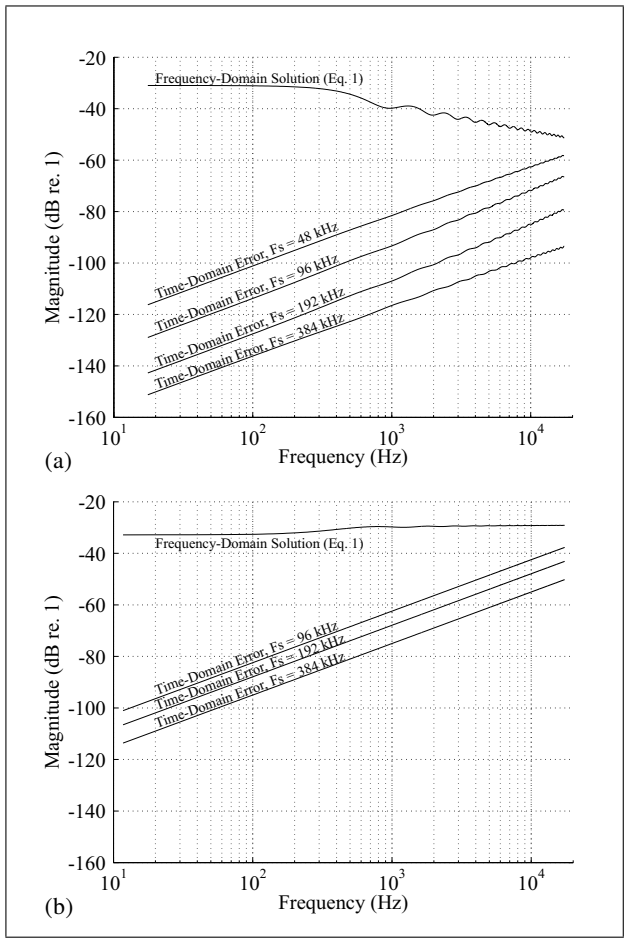

Figure 4. $|H_{diffr}(\omega)|$ calculated with the new formulation (equation 1) for the geometry in Figure 2, using edge endpoints $z_1 = 0$ m, $z_2 = 1$ m. Time-domain solutions computed for sampling frequencies 48 ((a) only), 96, 192, and 384 kHz have been transformed to the frequency domain using the FFT, and the error relative to the frequency-domain solution is shown. (a) Data for receiver R_1. (b) Data for receiver R_2.

presented. It has been shown to be identical to an analytical, contour-integral solution for the infinite wedge with a transformation of variables, and in addition the new formulation can be applied directly to finite edges. Numerical comparisons with the reference solution for the infinite wedge confirm the accuracy of the new method.

The presented solution permits the study of finite edges, but it is clear that a finite wedge generates first-order diffraction from a number of finite edges as well as higher-order diffraction components. Higher-order diffraction was studied in [7], but has not been discussed here. Previous studies have suggested that the use of only first-order diffraction is sufficient in the application of diffraction modeling to finite noise barriers [17] and room acoustics [3], but the current method should be extended to higher orders for further investigations. For the numerical integration of equation (1), the singularity can be avoided by applying an analytical approximation as discussed in section 2.2.

Acknowledgements

Parts of this research was funded by the Acoustics Research Centre project from the Research Council of Norway. Portions of the project were carried out during the third author's stay in Trond-

heim while he was affiliated with the Environmental Acoustics Laboratory, Kobe University, Kobe, Japan.

References

[1] T. M. Macdonald: A class of diffraction problems. Proc. Lond. Math. Soc. **14** (1915) 410–427.

[2] H. Medwin: Shadowing by finite noise barriers. J. Acoust. Soc. Am. **69** (1981) 1060–1064.

[3] R. R. Torres, U. P. Svensson, M. Kleiner: Computation of edge diffraction for more accurate room acoustics auralization. J. Acoust. Soc. Am. **109** (2001) 600–610.

[4] J. Vanderkooy: A simple theory of cabinet edge diffraction. J. Aud. Eng. Soc. **39** (1991) 923–933.

[5] R. S. Keiffer, J. C. Novarini: A time domain rough surface scattering model based on wedge diffraction: Application to low-frequency backscattering from two-dimensional sea surfaces. J. Acoust. Soc. Am. **107** (2000) 27–39.

[6] M. A. Biot, I. Tolstoy: Formulation of wave propagation in infinite media by normal coordinates with an application to diffraction. J. Acoust. Soc. Am. **29** (1957) 381–391.

[7] U. P. Svensson, R. I. Fred, J. Vanderkooy: An analytic secondary source model of edge diffraction impulse responses. J. Acoust. Soc. Am. **106** (1999) 2331–2344.

[8] J. Bowman, T. Senior: The wedge. – In: Electromagnetic and acoustic scattering by simple shapes. J. Bowman, T. Senior, P. Uslenghi (eds.). Hemisphere Publishing Corporation, New York, 1969, Kap. 6.

[9] A. D. Pierce: Acoustics. McGraw-Hill, New York, 1981.

[10] T. F. W. Embleton: Line integral theory of barrier attenuation in the presence of the ground. J. Acoust. Soc. Am. **67** (1980) 42–45.

[11] Y. Sakurai, K. Nagata: Sound reflections of a rigid plane and of the "live end" composed by those panels. J. Acoust. Soc. Jpn. **2** (1981) 5–14.

[12] P. Menounou, I. Busch-Vishniac, D. Blackstock: Directive line source model: A new model for sound diffration by half planes and wedges. J. Acoust. Soc. Am. **107** (2000) 2973–2986.

[13] U. P. Svensson, P. T. Calamia: Edge-diffraction impulse responses near specular-zone and shadow-zone boundaries. Acta Acustica united with Acustica **92** (2006) 501–512.

[14] D. Chu, T. Stanton, A. Pierce: Higher-order acoustic diffraction by edges of finite thickness. J. Acoust. Soc. Am. **122** (2007) 3177–3194.

[15] H. Medwin, E. Childs, G. M. Jebsen: Impulse studies of double diffraction: A discrete Huygens interpretation. J. Acoust. Soc. Am. **72** (1982) 1005–1013.

[16] J. P. Chambers, Y. H. Berthelot: Time-domain experiments on the diffraction of sound by a step discontinuity. J. Acoust. Soc. Am. **96** (1994) 1887–1892.

[17] Y. W. Lam, S. C. Roberts: A simple method for accurate prediction of finite barrier insertion loss. J. Acoust. Soc. Am. **93** (1993) 1445–1452.